Interaction of the Intrinsically Unstructured Phage λ N Protein with *Escherichia coli* NusA

Stefan Prasch, Sabine Schwarz, Anke Eisenmann, Birgitta M. Wöhrl, Kristian Schweimer,* and Paul Rösch

Lehrstuhl Biopolymere, Universität Bayreuth, Universitaetsstrasse 30, 95440 Bayreuth, Germany

ABSTRACT: N protein of the *Escherichia coli* phage λ (λN) is involved in antitermination, a transcription regulatory process that is essential for the expression of delayed early genes during phage lytic development. λN is an intrinsically unstructured protein that possesses three distinct binding sites interacting with the carboxy terminus of the *E. coli* host factor protein NusA, the viral *nutBoxB*-RNA, and RNA polymerase, respectively. Heteronuclear NMR experiments with λN(1−53) in complex with NusA(339−495) revealed that upon complex formation the λN-binding interface, λN(34−47), adopts a rigid structure. NMR data also indicate the induction of a weak helical structure in the *nutboxB* RNA-binding region λN(1−22) upon binding to NusA(339−495) even in the absence of RNA. Titration experiments of the λN(1−53)− *nutBoxB* RNA complex with NusA(339−495) revealed that the ternary complex can be described in terms of two structurally independent binary interactions. Furthermore, chemical-shift perturbation experiments with different NusA constructs and different λN peptides showed that only NusA(353−416) is involved in λN binding. We found that only one molecule of NusA(339−426) binds to one molecule of λN(1− 53). We also clarified the role of the λN-binding region and could show that N41−R47 also binds to NusA(339−495). Furthermore, we observe that λN(1−22) adopts a helical fold upon binding to NusA-(339−495), in agreement with one of the theoretical models of λN action.

One of the cornerstones of protein biochemistry is the structure−function paradigm, describing the relationship between the biological function of a protein and its three-dimensional structure (*1*). Recently, this point of view changed because of the increased analyses of intrinsically unstructured proteins (*2*). It is estimated that about 4.2% of all proteins in prokaryotes and 33.0% of all proteins in eukaryotes are intrinsically unstructured (*3*). These proteins are mainly involved in cell-cycle control and translational as well as transcriptional regulation (*3*). Transcriptional modulation of RNA polymerases (RNAPs) by intrinsically unstructured viral proteins is common in prokaryotes and eukaryotes; examples for such proteins are the λN protein (*4*, *5*), the phage HK022 Nun protein (*6*), and the human immunodeficiency virus (HIV)[1] Tat protein (*7*, *8*). All of these proteins are unstructured in the free state and employ similar mechanisms to regulate transcription in the host cells (*9*).

Transcriptional control by the regulation of RNA elongation is widely used in the microbial world. In the bacteriophage λ-*Escherichia coli* (*E. coli*) system, protein N of phage λ (λN) plays an essential role in transcriptional antitermination in the two phage early operons, which are critical for phage development. The inhibition of termination at intrinsic and Rho-dependent terminators by λN depends upon the recognition of an RNA element called *nut* (N utilization) on the nascent phage transcript. This RNA element consists of two parts, *nutBoxA* and *nutBoxB*. N and NusA together with the *nutBoxB* sequence are sufficient to induce effective antitermination in vitro at many terminators located within a few hundred base pairs downstream of a *nutBoxB* site (*10−13*). Highly efficient, processive N-mediated antitermination also requires *E. coli* transcription elongation factors NusA, NusB, NusG, and NusE (S10), as well as *nutboxA* (*12−15*). After this complex has been formed, it leads to efficient in vitro and in vivo suppression of terminators located thousands of base pairs downstream of the *nut* site (*16*, *17*).

The key component of the antitermination complex is the highly basic 107 amino acid λN protein, which is largely unfolded in solution (*4*, *5*). λN consists of three functionally distinct regions with different interaction partners: M1−N22 binds the *nutBoxB* RNA, N34−R47 binds the carboxy-terminal part of *E. coli* NusA, R73−I107 forms the RNA polymerase (RNAP) binding region (*5*, *18*).

The region M1−N22 of λN, called the arginine-rich motif (ARM), binds to the *nutBoxB* RNA hairpin with an affinity of ∼10^{-9} M (*19−21*). The structure of the ARM region and *nutBoxB* RNA has already been solved by nuclear magnetic resonance (NMR) spectroscopy. Upon RNA binding, the ARM region of λN adopts a stable α-helical conformation (*22*, *23*). The complex formation enforces a GNRA-type

* To whom correspondence should be addressed: Lehrstuhl Biopolymere, Universität Bayreuth, Universitaetsstrasse 30, 95440 Bayreuth, Germany. Telephone: +49-921-553543. Fax: +49-921-553544. E-mail: kristian.schweimer@uni-bayreuth.de.

[1] Abbreviations: CD, circular dichroism; NMR, nuclear magnetic resonance; λN, protein N of phage λ; HhH, helix hairpin helix; ARM, arginine-rich motif; AR, acidic repeat; AR1, NusA(353−416); AR2, NusA(431−490); *E. coli*, *Escherichia coli*; HIV, human immunodeficiency virus; YUH, yeast ubiquitin hydrolase; HSQC, heteronuclear single-quantum coherence; NOE, nuclear Overhauser effect; NOESY, NOE spectroscopy.

tetraloop fold of the five nucleotide *nutBoxB* RNA loop with one base extruded. W18 then stacks on the top of the tetraloop fold and extends the RNA π stack by one residue. Randomized mutagenesis studies revealed that the complex interface is the principal determinant of functional antitermination (*24*).

The region N34−R47 interacts with the carboxy-terminal part of *E. coli* NusA (*5*). N34−R47 binds to NusA with an affinity of 70 nM (*21, 24*), nearly 2 orders of magnitude weaker than the ARM region binds to *nutBoxB* RNA. The NMR structure of the carboxy terminus of NusA (NusA339−495) in the free state showed that *E. coli* NusA(339−495) consists of two separate domains acidic repeat (AR)1, NusA-(353−416). and AR2, NusA(431−490) (*25*), with either one adopting a compact helix−hairpin−helix (HhH)₂ fold (*26*). The two domains are connected by a 14-residue flexible linker region (*26*). The three-dimensional structure of the complex of λN and the carboxy-terminal part of *E. coli* NusA has been solved by X-ray crystallography (*27*). It shows only interactions between AR1 and N34−L40. The second part of the λN-binding site, N41−R47, could not be detected in the electron-density map. Furthermore, the X-ray data reported a 2:1 stoichiometry of AR1/λN(34−47) (*27*). Isothermal titration calorimetry (ITC) and mutational studies suggested, however, that only the 1:1 complex between NusA and λN is biologically relevant (*27*). On the basis of these results, it was suggested that, in full-length NusA, N41−R47 binds to AR2 (*27*).

The sequence of steps leading to the formation of the complex of λN, NusA, and RNAP is still unclear. One model proposes that NusA binds to RNAP after the initiation process. Immediately after the *nutBoxB* RNA leaves the RNAP, N binds to the RNA tetraloop and is recruited to the transcription elongation complex. Complex formation transforms the RNAP into a termination-resistant transcription complex (*5, 16, 28−30*). In an alternative model, λN, NusA, and RNAP associate prior to the exit of RNAP from the *nut* site. λN is then able to scan the nascent RNA for the *nutBoxB* signal and finally binds to it, forming a processive antitermination complex (*24*).

In this work, we studied the complex of intact NusA(339−495) with λN(1−53) by multidimensional, heteronuclear nuclear magnetic resonance (NMR) spectroscopy to clarify the role of AR1 and AR2 and to further investigate details of the λN−NusA interaction as an essential building block of a functional antitermination complex.

MATERIALS AND METHODS

Expression and Purification of λN(1−53) and NusA(339−495). A synthetic gene containing the λN(1−53) DNA sequence adapted to the *E. coli* codon usage was cloned into the expression vector pTKK 19 (*31*). *E. coli* strain BL21 DE3 (Novagen) was transformed with the resulting plasmid. The expressed protein consisted of an amino-terminal deca-His-tag fused to ubiquitin from *Saccharomyces cerevisiae* followed by λN(1−53). For double labeling, cells were grown in M9 minimal medium supplemented with $^{15}NH_4Cl$ and 0.2% ^{13}C D-glucose as the sole nitrogen and carbon sources, respectively (*32*).

The recombinant protein was purified by nickel-affinity chromatography (5 mL His-trap chelating column, GE Health

Care) under denaturing conditions, using a buffer containing 20 mM Tris/HCl at pH 7.95, 200 mM imidazol, 500 mM NaCl, and 6 M urea. After the protein was bound to the column, urea was removed by decreasing the urea concentration slowly over 20 column volumes. The protein was eluted with a buffer containing 20 mM Tris/HCl at pH 7.9, 200 mM imidazole, and 500 mM NaCl. Fractions containing the protein were dialyzed against 50 mM Tris/HCl at pH 7.9, 100 mM NaCl, and 1 mM β-mercaptoethanol. Ubiquitin was cleaved off using yeast ubiquitin hydrolase (YUH) (1 mg/mL) (*31*). The λN(1−53) peptide was further purified by reversed-phase HPLC using a C-18 column (Macherey and Nagel, Germany) with a constant gradient of 80% acetonitrile/water and 0.1% TFA (v/v). The molecular mass of λN-(1−53) was checked by SDS−PAGE and ESI−MS.

A synthetically produced gene adapted to the *E. coli* codon usage harboring the AR1 domain of NusA(339−426) was cloned via the *Nde*I and *Bam*HI restriction sites into the *E. coli* expression vector pET19b (Novagen). The plasmid was transferred into the *E. coli* strain BL21 (DE3) (Novagen). The resulting soluble recombinant protein contained an N-terminal deca-His tag. For ^{15}N and ^{13}C labeling, cells were grown in M9 minimal medium with $^{15}NH_4Cl$ and ^{13}C glucose as the sole nitrogen and carbon sources, respectively (*32*).

To purify NusA(339−426), bacterial cell pellets were lysed by sonication in 20 mM $NaPO_4$ at pH 7.4, 0.5 M NaCl, and 1 mM dithiothreitol (DTT). After centrifugation, the supernatant was loaded onto a Ni-ion-affinity column (His-trap chelating, GE Health Care) and eluted by applying an imidazole step gradient. Peak fractions containing NusA-(339−426) were dialyzed against 50 mM Tris/HCl at pH 8.0, 150 mM NaCl, and 1 mM DTT. After dialysis, the N-terminal deca-His tag was cleaved off using PreScission protease (0.8 unit/100 μg protein). The cleaved NusA(339−426) was dialyzed against 50 mM Tris/HCl at pH 7.4 and 1 mM DTT and further purified via a QXL column (GE Health Care) by a NaCl step gradient in the same buffer with up to 1 M NaCl. The eluted fractions containing NusA(339−426) were concentrated with Vivaspin concentrators (Vivascience, MWCO 5000 Da).

Unlabeled and ^{15}N-labeled NusA(339−495) was purified as described previously (*26*). Chemically synthesized λN-(34−47) peptide containing blocked endgroups was obtained from Coring (Gernsheim, Germany).

NMR Sample Preparation. NMR samples consisted of 0.5−1.5 mM λN(1−53) in 10 mM KPO_4 at pH 6.8, 50 mM NaCl, 0.02% sodium azide, and 10% D_2O. Titration of ^{15}N-labeled λN(1−53) was done by gradually adding up to a 5-fold molar excess of unlabeled NusA(339−495). NMR experiments for characterizing λN(1−53) in the NusA-bound state were performed in the presence of a 2-fold excess of NusA(339−495).

NMR Spectroscopy. NMR spectra were recorded on Bruker Avance 400 MHz, DRX 600 MHz, Avance 700 MHz, and Avance 800 MHz spectrometers with either room temperature or cryogenic-cooled triple-resonance probes equipped with pulsed field-gradient capabilities. The sample temperature was either 298 K for titration experiments or 308 K in the case of the assignment experiments for doubly labeled λN(1−53) bound to NusA(339−495) to improve the NMR spectra. However, characteristic chemical-shift changes were independent of the temperature. For assignment of the λN-

(1−53) resonances in the free and NusA(339−495)-bound states, standard double- and triple-resonance experiments were performed (*33, 34*). The steady-state $\{^1H\}^{15}N$ nuclear Overhauser enhancement (NOE) experiment was recorded using water flipback pulses and a binomial 3-9-19 watergate for water suppression (*33*). A relaxation delay of 6 s was employed. In the saturated subspectrum, protons were saturated by applying a series of 120° pulses with a 5 ms interval during individual pulses for the final 3 s of the relaxation delay. $\{^1H\}^{15}N$ steady-state NOEs were expressed as intensity ratios of the corresponding signals in the saturated and unsaturated subspectra. Amide resonances of NusA-(339−426) in the free and λN(1−53)-bound states were assigned by comparing the chemical shifts and NOE patterns in 3D ^{15}N-edited NOE spectroscopy (NOESY)−heteronuclear single-quantum coherence (HSQC) experiments with the corresponding data of NusA(339−495).

The dissociation constant K_D was determined from the changes of chemical shifts of ^{15}N-labeled λN(1−53) observed in an $^1H,^{15}N$ HSQC after gradual addition of the corresponding unlabeled binding partner [NusA(339−495) or λN peptides]. Changes of chemical shifts of signals in the fast-exchange limit were fitted to the following equation for a two-state model:

$$\delta_{obs} = \delta_P + (\delta_{PL} - \delta_P)\left[\frac{\{K_D + (1 + r)[P]_0\}}{2[P]_0} - \frac{\sqrt{(K_D + (1 + r)[P]_0)^2 - 4[P]_0^2 r}}{2[P]_0}\right]$$

δ_{obs}, δ_P, and δ_{PL} are the chemical shifts for the actual mixture, the free λN(1−53) peptide, and the completely bound peptide, respectively. $[P]_0$ is the total concentration of λN-(1−53), and r describes the NusA(339−495)/λN(1−53) ratio.

Normalized chemical-shift changes of the amide resonances were expressed as

$$\Delta\delta_{norm} = \sqrt{\Delta\delta(^1H)^2 + (0.1\Delta\delta(^{15}N))^2}$$

$\Delta\delta(X)$ represents the chemical-shift difference of spin X between free and bound states. Normalized chemical-shift changes larger than 0.04 ppm were considered as significant (*35*).

RESULTS AND DISCUSSION

Free λN(1−53) Peptide and Its Interactions with boxB and NusA. Multidimensional heteronuclear NMR spectroscopy yielded assignments for all ^1H, ^{13}C, and ^{15}N resonances of free λN(1−53), except for some arginine side chains in the ARM region λN(1−22). For these residues, severe spectral overlap made an unambiguous assignment impossible. In agreement with previous circular dichroism (CD) and NMR spectroscopic measurements (*21*), the narrow chemical-shift dispersion in $^1H,^{15}N$ HSQC (Figure 1A) as well as in $^1H,^{13}C$ HSQC spectra indicates structural disorder of the peptide (Figure 1A) (*36, 37*). $\{^1H\}^{15}N$ steady-state NOE measurements at 14.1 T resulted in negative signal intensities or missing signals in the saturated subspectrum compared to the unsaturated subspectrum (Figure 1B). Thus, the intensity ratio of the saturated versus the nonsaturated
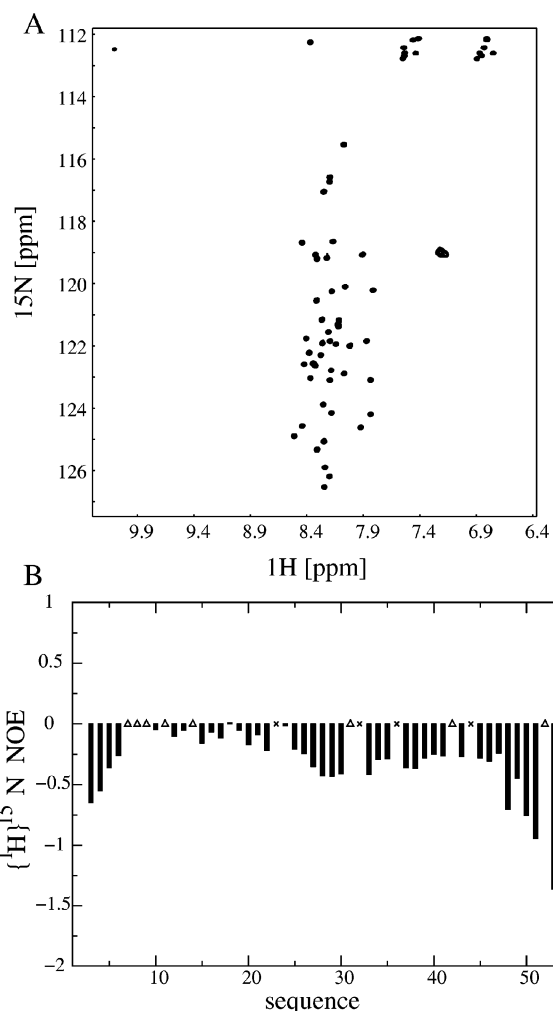

FIGURE 1: Free λN(1−53) peptide. $^1H,^{15}N$ HSQC spectrum (800 MHz) (A) and $\{^1H\}^{15}N$ NOE at 600 MHz of free λN (1−53) peptide (B). The low dispersion together with the $\{^1H\}^{15}N$ NOE values below 0 characterize the free λN(1−53) peptide as an unstructured highly flexible peptide chain.

subspectrum is 0 or less for all residues, clearly pointing to a high flexibility of λN(1−53). Less negative values for the RNA-binding region, R10−A20, may be interpreted in terms of decreased flexibility of this region as compared to the rest of the peptide.

Interaction Interfaces in the Ternary Complex Are Similar to That of the Binary Complexes. The interaction between λN(1−53), *nutBoxB* RNA, and NusA(339−495) was monitored by observing chemical-shift changes of ^{15}N-labeled λN-(1−53) after the gradual addition of unlabeled *nutBoxB* RNA and/or NusA(339−495) in $^1H,^{15}N$ HSQC spectra (Figure 2). On the basis of the titration experiments alone, it was not possible to completely assign the λN(1−53) resonances of the respective complexes because some nuclei showed slow and intermediate exchange behavior during the titration. However, using multidimensional heteronuclear NMR spectra, all resonances of $^{13}C,^{15}N$-labeled λN(1−53) in the complex with NusA(339−495) could be assigned, with the exception of the backbone resonances of R11, R35, and P36 and a few side-chain resonances of longer amino acids.

Nearly all $^1H^N$ and ^{15}N resonances of λN(1−53) change upon binding of the peptide to NusA(339−495), the most prominent changes occurring in the region I37−K45 (Figure 3A). This region has been implicated previously in complex
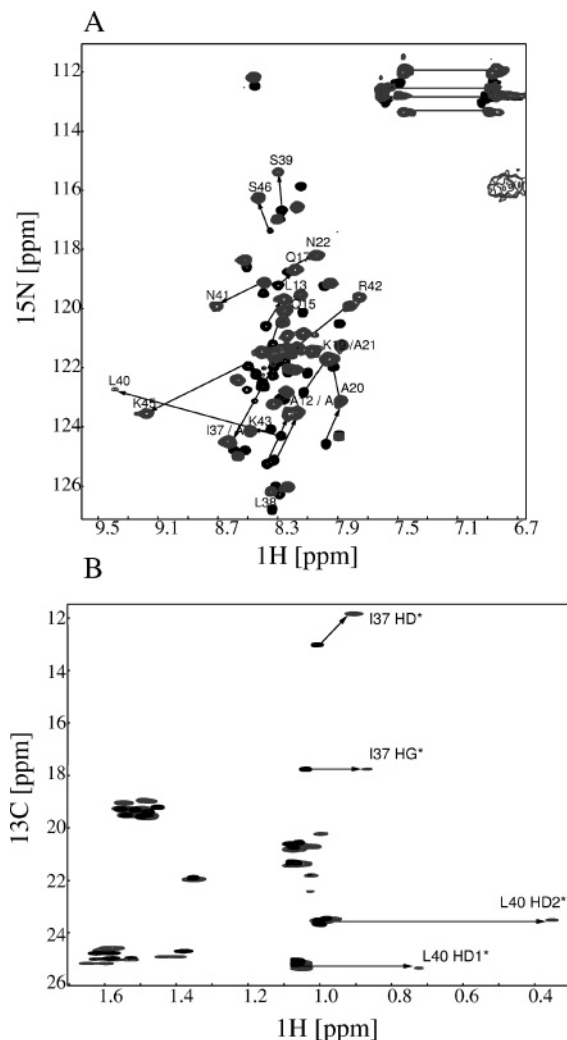
FIGURE 2: Interaction of λN(1−53) and NusA(339−495). Overlay of ¹H,¹⁵N HSQC (A) and methyl region of ¹H,¹³C constant time HSQC (B) of free ¹⁵N,¹³C-labeled λN(1−53) peptide (black) and in the presence of 2 equiv of unlabeled NusA(339−495) (gray). Resonances with remarkable changes of chemical shifts are labeled.
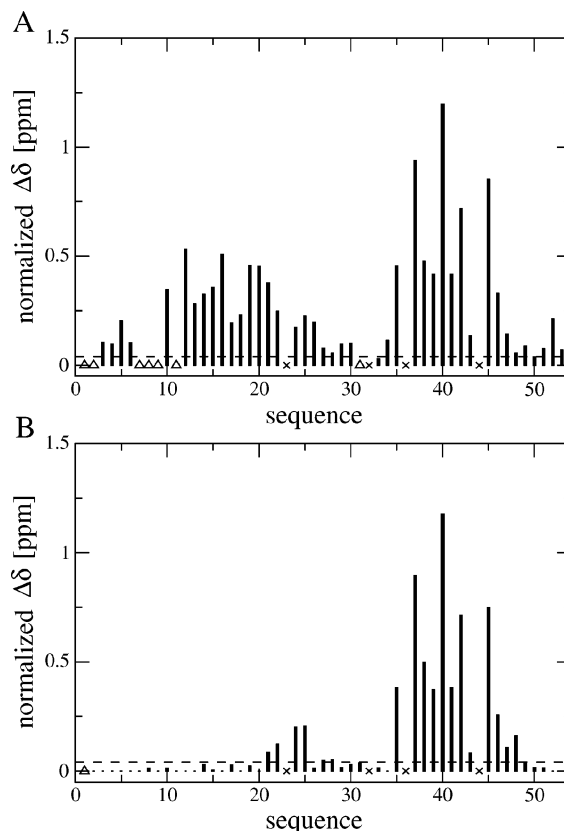

FIGURE 3: Backbone chemical-shift changes upon binding. (A) Investigation of the binary system. Changes of chemical shifts of λN(1−53) after binding to NusA(339−495) as a function of the primary sequence. Normalized chemical-shift changes larger than 0.04 ppm were considered significant (*35*) (×, proline; △, missing residues). (B) Investigation of the ternary system. Differences of amide chemical shifts of λN(1−53) complexed to *nutBoxB* RNA in the presence and absence of NusA(339−495). The lack of chemical-shift changes in the ARM region of λN (M1−N22) complexed with *nutBoxB* RNA after the addition of NusA(339−495) indicates no ternary interaction, while the similar chemical-shift changes for residues I37−K45 point to the same structural binding mode between λN(1−53) and NusA(339−495) in the presence or absence of *nutBoxB* RNA.

formation (*5*). Surprisingly, remarkable changes in the presence of NusA(339−495) could not only be detected within the expected binding region but also in the RNA-binding ARM region (residues M1−N22) of λN(1−53).

To investigate whether changes in the ARM region could be observed upon the addition of NusA(339−495) in the presence of its known binding partner *nutBoxB* RNA, we gradually added unlabeled NusA(339−495) to a complex of ¹⁵N-labeled λN(1−53) and *nutBoxB* RNA. Because changes could only be observed in the expected NusA-binding region, N34−R47, of λN(1−53) (Figure 3B), we conclude that in the binary NusA(339−495)−λN(1−53) complex as well as in the ternary NusA(339−495)−λN(1−53)−*nutBoxB* RNA complex the conformation of residues N34−R47 of λN(1−53) is virtually identical and thus is not influenced by *nutBoxB* RNA to a measurable extent.

ARM Region of λN(1−53) Possesses Helix Propensity That Can Be Enhanced by NusA(339−495). Secondary chemical shifts of backbone ¹³Cα and ¹³C′ resonances are related to the peptide secondary structure (*36*). We referenced the chemical shifts of bound λN(1−53) to the values of free λN-(1−53) rather than to published random-coil data, because the negative or close to 0 {¹H}¹⁵N steady-state NOEs at 14.1

T of the free peptide indicate high flexibility of this peptide on the pico−nanosecond time scale and thus make it an ideal internal standard. Upon NusA(339−495) binding, notable changes for ¹³Cα and ¹³C′ can be observed in the amino-terminal RNA-binding region and around residues I37−K45 (Figure 4), in good agreement with changes of the ¹HN and ¹⁵N chemical shifts (Figure 3).

In particular, downfield shifts which are characteristic for helical secondary-structure formation are observed for ¹³Cα and ¹³C′ of the λN ARM region after NusA(339−495) binding (Figure 4). The helical tendency is less pronounced for ¹³Cα but can be clearly seen for the ¹³C′ spins (Figure 4A). The chemical-shift changes extend over more than 13 amino acids, corresponding to three helical turns (Figure 4B). These changes indicate an increase of the population of the helical secondary structure for the RNA-binding region of λN(1−53) in the NusA(339−495)−λN(1−53) complex even in the absence of *nutBoxB* RNA. Further evidence for the existence of an α helix in the binary complex is the predominance of characteristic medium-range NOEs, such as [dαN(*i*, *i* + 3)] and [dαβ(*i*, *i* + 3)] (*38*, *39*). These NOE patterns could be found for at least six residues (E15, A16,
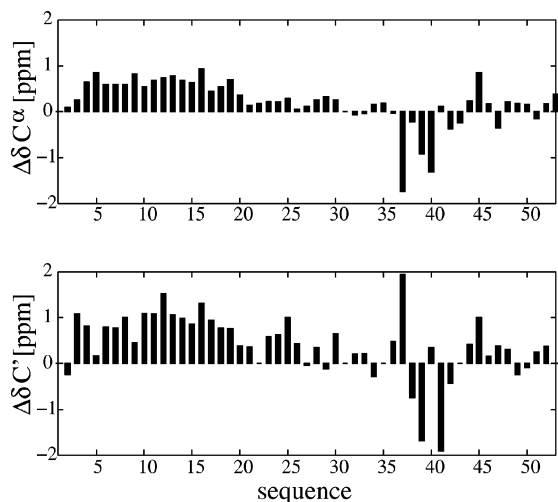
FIGURE 4: $^{13}C^{\alpha}$ and $^{13}C'$ chemical-shift changes upon binding. Changes of $^{13}C^{\alpha}$ and $^{13}C'$ chemical shifts of $\lambda N(1-53)$ peptide after binding to NusA(339−495). Chemical-shift changes for $^{13}C^{\alpha}$ and $^{13}C'$ larger than 0.14 ppm were considered significant because of the spectral resolution. The changes of chemical shifts to a lower field for both nuclei indicates an increase of the propensity of the helical secondary structure for the ARM region after binding of $\lambda N(1-53)$ to NusA(339−495) even in the absence of *nutBoxB* RNA.
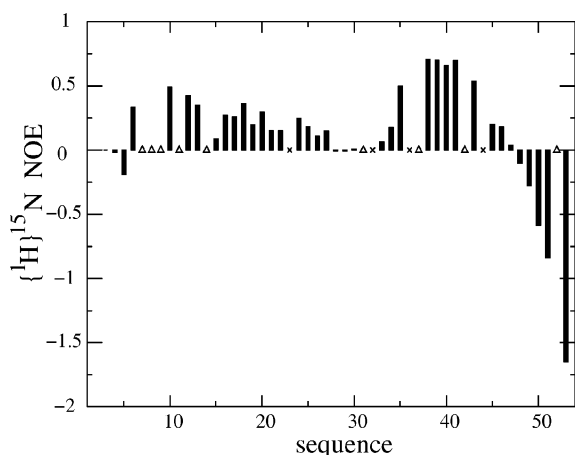

FIGURE 5: $\{^1H\}^{15}N$ NOE in the bound state. $\{^1H\}^{15}N$ steady-state NOE (600 MHz) of $\lambda N(1-53)$ peptide in the presence of 2 equiv of NusA(339−395). Typical ranges (>0.65) found in rigid-folded polypetide chains are shown by the dashed line (*40*).

E17, W18, K19, and A20) in the carboxy-terminal part of the ARM motif.

Additionally, we measured the $\{^1H\}^{15}N$ NOE at 14.1 T of $\lambda N(1-53)$ in the NusA(339−495)−$\lambda N(1-53)$ complex (Figure 5). In comparison to the free state, positive NOE values can be found for the region T5−A20. This increase can mainly be attributed to the enhanced overall tumbling time after complex formation and reflects flexibility on the pico−nanosecond time scale in the bound state. However, the values did not reach the typical range (>0.65) found in folded and rigid polypeptide chains (*40*). Therefore, a substantial flexibility on the pico−nanosecond time scale persists in the ARM region of λN even after binding to NusA.

N34−R47 of $\lambda N(1-53)$ Binds to NusA(339−495) with a Well-Defined Structure. $\lambda N(1-53)$ binds to NusA(339−495) independently of *nutBoxB* RNA, and the relevant binding site includes residues N34−R47 (*21*, *24*). Upon NusA(339−495) binding, the $^1H,^{15}N$ HSQC spectrum of $\lambda N(1-53)$

exhibits significant changes of chemical shifts, e.g., L40 (1.2 ppm normalized chemical-shift change) and K45 (0.6 ppm). Furthermore, this region also exhibits the largest chemical-shift changes for $^{13}C^{\alpha}$ and $^{13}C'$ resonances (Figure 4) and considerable shifts of the methyl groups to a higher field (Figure 2B). High-field shifts of methyl groups are typically observed in hydrophobic cores of proteins or at binding interfaces (*38*, *39*) and indicate a structurally defined complex formation. The chemical-shift changes for N34−L40 are thus consistent with results from X-ray crystallography, showing that these residues are involved in complex formation. Particularly, analysis of the crystal structure suggests that the upfield shifts of the L40 methyl resonances are due to a ring current effect caused by F369 of NusA (*27*).

In addition, the resonances of residues N41−K45 show chemical-shift changes, most prominent in K45 ($^1H^N$, 0.74 ppm), suggesting the involvement of these residues in complex formation, in agreement with data obtained with different deletion mutants of λN (*5*). In that study, the peptide M1−R47 shows stronger binding affinity to NusA(1−495) than M1−P44. This finding together with the large chemical-shift change of K45 in our analyses implies an interaction of N41−K45 with the carboxy-terminal region of NusA, an interaction that could not be observed in the X-ray crystallographic studies because no electron density could be observed for N41−K45.

In contrast to A3−N22, the region N34−R47 shows no typical chemical-shift pattern for a regular secondary structure, in good agreement with the crystal structure, where N(34−40) adopts an extended conformation. The steady-state $\{^1H\}^{15}N$ NOE suggests the peptide backbone to be rather rigid for residues I37−K43 (Figure 5), with $\{^1H\}^{15}N$ NOEs values in the range of 0.5−0.7, which characterize this region as the most rigid part of $\lambda N(1-53)$ after NusA-(339−495) binding. Indeed, these values are close to those typically found in structured regions of proteins, where an NOE cutoff value of 0.65 at 14.1 T is commonly used to distinguish isotropic tumbling and conformational exchange (*40*). This indicates the formation of a well-defined structure for residues I37−K43 in the complex with NusA(339−495). The gradual decrease of the $\{^1H\}^{15}N$ NOE values toward the carboxy terminus associated with an increase of flexibility may explain the absence of theses residues in the X-ray crystallographic electron-density map.

$\lambda N(1-53)$ Interacts Only with AR1. It was shown previously by X-ray crystallography that the peptide-spanning residues N34−R47 of λN bind to AR1, and only residues N34−L40 are visible in the electron density (*27*). Although the AR2 domain was not present in the crystal, it was suggested that it interacts with residues N41−R47 of λN in the intact system. This model was based on three observations. First, peptide N34−R47 of λN has a 3-fold higher affinity to NusA than peptide K31−K43 of λN. Second, the λN sequences N34−L40 (NRPILSL) and N41−R47 (NRK-PKSR) are highly similar. Third, NusA(339−495) consists of two structurally equivalent domains (*27*).

Our titration experiments using ^{15}N-labeled $\lambda N(1-53)$ together with NusA(339−495) also indicate an interaction of NusA and the λN region N41−R47. From these results alone, however, we cannot conclusively state whether AR2 is directly involved in binding. To better define the binding region of NusA(339−495), additional titrations using ^{15}N-

labeled NusA(339−495) and unlabeled λN peptides were performed. To avoid unspecific charge−charge interactions between the negatively charged NusA and the positively charged ARM region of λN(1−53), synthetic peptides spanning residues N34−R47 and N41−R47 of λN were used. Up to a 2-fold excess of N34−R47, only resonances of ^{15}N-labeled AR1 residues changed their position in the ^{1}H,^{15}N HSQC spectra (Figure 6A), clearly demonstrating that only AR1 is involved in high-affinity binding to N34−R47 of λN. Chemical-shift changes in AR2 could only be observed after saturation of AR1 with λN(34−47), pointing to an unspecific interaction between positively charged N34−R47 of λN (+5) and negatively charged AR2 (−9). In a second experiment, we titrated the peptide λN(41−47) up to a 5-fold excess to ^{15}N-labeled NusA(339−495). With the exception of residues V372, G377, S379, and L398, all located in AR1 (Figure 6B), no significant changes were observed.

The chemical-shift changes of amide resonances of NusA-(339−495) during the titration with λN(34−47) fit well to a two-state model (Figure 6C). The intersection of the two straight lines in the titration profile of ^{15}N-labeled NusA-(339−495) indicates a 1:1 ratio of NusA(339−495) and λN-(34−47), implying that a single NusA(339−495) molecule binds to one λN(34−47) molecule (Figure 6C). The K_D value estimated for the peptide complex from the titrations was in the range of 3.7 to 5.0 μM, comparable to values measured with ITC [3.55 μM (27)].

Titrations of ^{15}N-labeled λN(1−53) with NusA(339−495) allowed for the observation of chemical-shift changes with fast-exchange behavior for resonances located in the RNA-binding region of λN, and a K_D of 10−20 μM could be estimated. Although the resonances used for K_D determination lie outside the binding region for NusA(339−495), the observed K_D is similar and therefore confirms the former measurement. The chemical-shift changes of residues located in the ARM region of λN(1−53) after NusA binding were attributed to an increase of helical secondary structure, with the K_D value therefore reflecting the induction of the secondary structure outside the binding region rather than the direct interaction. Because both measured K_D values are nearly identical, the structural transition of the ARM region on NusA(339−495) binding correlates directly with the binding. Our NMR data indicate that residues N34−R47 are involved in binding to NusA(339−495), whereas residues N41−R47 probably do not contribute much to the binding energy. Differences in the K_D values of N34−R47 and K31−K43 are negligible, suggesting that the region N41−R47 contributes little to the binding energy (27). The differences in the K_D values measured with ITC and NMR, which are both in the same range, compared to values measured with fluorescence can be due to different salt conditions (21, 24, 27). Moreover, the high protein concentration required for the NMR experiments prohibits accurate K_D measurements in the low micromolar range, and the resulting K_D values reflect an upper limit only.

These titration experiments clearly demonstrate that all chemical-shift changes observed for NusA(339−495) are located in the region of AR1, strongly suggesting that only AR1 is the relevant part of the carboxy-terminal region of NusA for binding to λN. Nevertheless, these experiments do not prove whether AR1 alone is responsible for all chemical-shift changes observed for λN(1−53). To answer
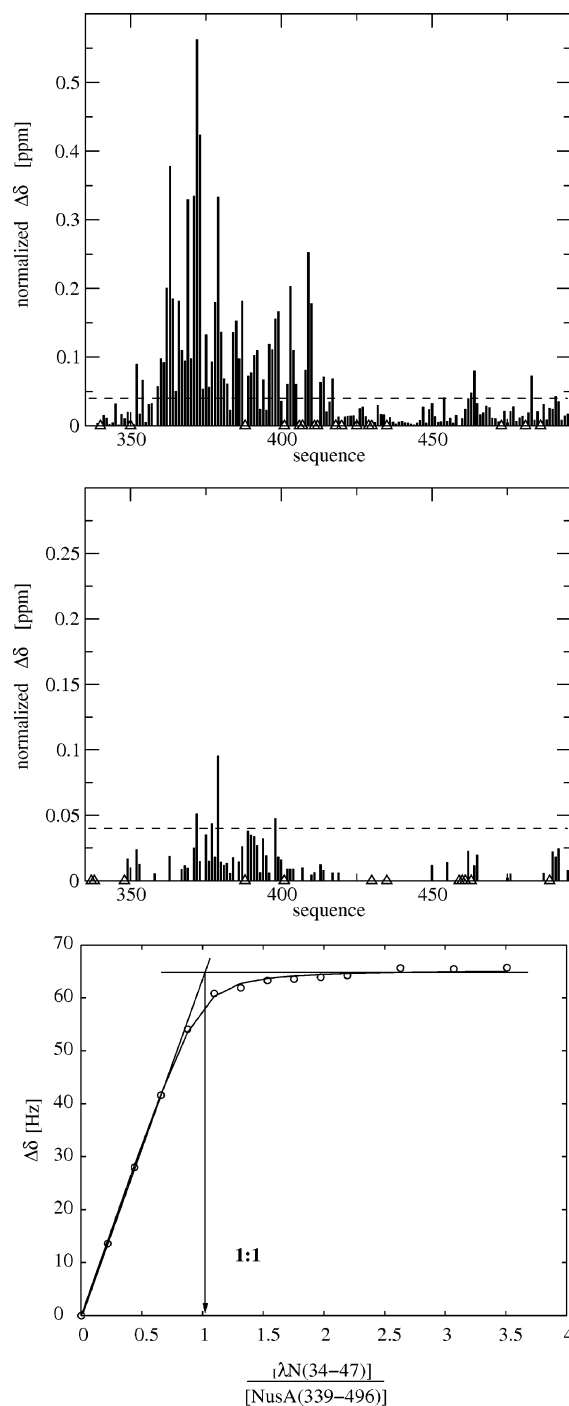

FIGURE 6: Titration of ^{15}N NusA(339−495) with λN peptides. Normalized chemical-shift changes of ^{15}N NusA(339−495) in the presence of a 2-fold molar excess of unlabeled λN(34−47) (A) or in the presence of a 3-fold molar excess of unlabeled λN(41−47) (B). Normalized chemical-shift changes larger than 0.04 ppm (- - -) were considered significant (35). (△, missing signals or overlap). The lack of chemical-shift changes in the AR2 domain of NusA(339−495) after the addition of λN peptides indicate that AR2 is not involved in binding. (C) Stoichiometric titration of ^{15}N NusA (339−495) with λN(34−47) probed by NMR chemical-shift changes. The intersection at a ratio of 1:1 implies that one NusA-(339−495) molecule binds to one λN(34−47) molecule. L393 was used as an example. The determined K_D value is in the range of 9.8 μM.

this question, NusA(339−426), containing AR1 only, was expressed, purified, and used for additional NMR experiments. Using ^{15}N-labeled NusA(339−426) in a titration with unlabeled λN(1−53), chemical-shift changes identical to
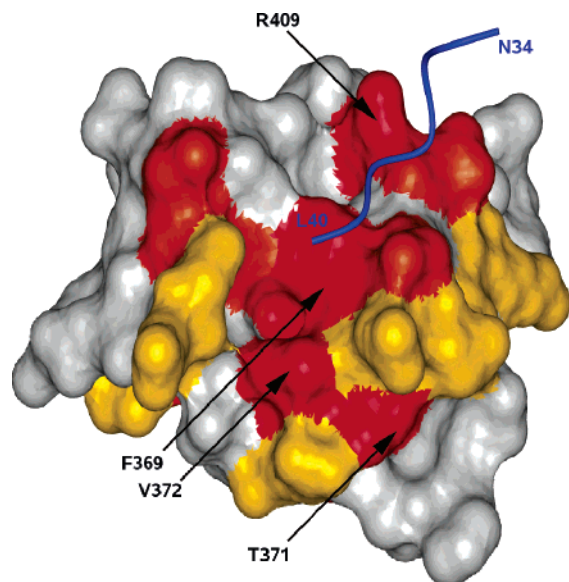
FIGURE 7: Mapping of the chemical-shift perturbations. Surface representation of the X-ray structure of NusA (339−426) in the presence of λN(34−40) (*27*). The backbone of λN(34−40) is shown in blue. The solvent-accessible surface of NusA (339−426) is shown in different colors according to the normalized chemical-shift perturbations (Δ_{norm}): gray, Δ_{norm} < 0.09 ppm; yellow, 0.09 ppm < Δ_{norm} < 0.15 ppm; orange, 0.15 ppm < Δ_{norm} < 0.20 ppm; and red, 0.20 ppm < Δ_{norm}. Amino acids with the largest chemical-shift perturbations are indicated by arrows. The representation was produced with MOLMOL (*42*).

those already found for NusA(339−495) were observed (see Figure S1 in the Supporting Information). This unambiguously demonstrates that AR1 is the sole binding domain for λN(1−53). Additionally, the titration of ^{15}N-labeled λN(1−53) with unlabeled NusA(339−426) produced the same chemical-shift changes as the initial experiment with NusA-(339−495). The prominent chemical-shift changes of the residues I37−K45 were present as well as the changes in the ARM region (see Figure S2 in the Supporting Information). It is clearly shown that AR1 alone causes the changes in the NMR spectrum of λN(1−53) for the residues of the known binding region (N34−R47) and for the residues located in the ARM region.

Mapping the observed chemical-shift changes onto the surface of the crystal structure of the complex of AR1 with λN(34−47) (Figure 7) gives further insight into the binding interface. Significant chemical-shift changes are found for the already known interface between AR1 and the region N34−L40. Additionally, large chemical-shift changes observed for F369, T371, V372, and L373 indicate the region of AR1 interacting with the additional residues of λN, N41−R47. This region involves the carboxy-terminal part of helix 2 and the hairpin between helices 4 and 5.

Recent low-temperature studies of *nutBoxB* RNA showed a conformational equilibrium of this RNA between the conformation found in the λN-bound state and other conformations (*41*). It is demonstrated that the amount of free RNA in the bound conformation is essential for binding, suggesting that enhancing the population of the binding conformation is a mechanism to facilitate complex formation. Short λN peptides were described to populate the binding helical conformation at least to a small amount (*19*). Our structural NMR studies describe the increased population of

the helical conformation in the ARM region of λN(1−53) after binding of λN(1−53) to NusA AR1. In analogy to the situation described for *nutBoxB* RNA (*41*), it is likely that the preformation of the *nutBoxB*-bound λN conformation in the ARM region on NusA-binding facilitates the recognition of the *nutBoxB* RNA. This could well be interpreted as lending additional support to the recently proposed model that λN binds to NusA before the *nutBoxB* RNA interaction (*24*).

SUPPORTING INFORMATION AVAILABLE

Overlay of ^{1}H,^{15}N HSQC spectra of ^{15}N-labeled NusA-(339−426) in the absence and presence of λN(1−53) (Figure S1) and overlay of ^{1}H,^{15}N HSQC spectra of ^{15}N-labeled λN-(1−53) in the absence and presence of NusA(339−426) (Figure S2). This material is available free of charge via the Internet at http://pubs.acs.org.

REFERENCES

1. Uversky, V. N. (2002) Natively unfolded proteins: A point where biology waits for physics, *Protein Sci. 11*, 739−756.
2. Dyson, H. J., and Wright, P. E. (2005) Intrinsically unstructured proteins and their functions, *Nat. Rev. Mol. Cell. Biol. 6*, 197−208.
3. Fink, A. L. (2005) Natively unfolded proteins, *Curr. Opin. Struct. Biol. 15*, 35−41.
4. van Gilst, M. R., and von Hippel, P. H. (2000) Quantitative dissection of transcriptional control system: N-Dependent antitermination complex of phage λ as regulatory paradigm, *Methods Enzymol. 323*, 1−31.
5. Mogridge, J., Legault, P., Li, J., van Oene, M. D., Kay, L. E., and Greenblatt, J. (1998) Independent ligand-induced folding of the RNA-binding domain and two functionally distinct antitermination regions in the phage λ N protein, *Mol. Cell 1*, 265−275.
6. Faber, C., Scharpf, M., Becker, T., Sticht, H., and Rosch, P. (2001) The structure of the coliphage HK022 Nun protein-λ-phage boxB RNA complex. Implications for the mechanism of transcription termination, *J. Biol. Chem. 276*, 32064−32070.
7. Willbold, D., Rosin-Arbesfeld, R., Sticht, H., Frank, R., and Rosch, P. (1994) Structure of the equine infectious anemia virus Tat protein, *Science 264*, 1584−1587.
8. Bayer, P., Kraft, M., Ejchart, A., Westendorp, M., Frank, R., and Rosch, P. (1995) Structural studies of HIV-1 Tat protein, *J. Mol. Biol. 247*, 529−535.
9. Brigati, C., Giacca, M., Noonan, D. M., and Albini, A. (2003) HIV Tat, its targets and the control of viral gene expression, *FEMS Microbiol. Lett. 220*, 57−65.
10. Whalen, W., Ghosh, B., and Das, A. (1988) NusA protein is necessary and sufficient in vitro for phage λ N gene product to suppress a rho-independent terminator placed downstream of nutL, *Proc. Natl. Acad. Sci. U.S.A. 85*, 2494−2498.
11. Whalen, W. A., and Das, A. (1990) Action of an RNA site at a distance: Role of the nut genetic signal in transcription antitermination by phage-λ N gene product, *New Biol. 2*, 975−991.
12. Mason, S. W., Li, J., and Greenblatt, J. (1992) Host factor requirements for processive antitermination of transcription and suppression of pausing by the N protein of bacteriophage λ, *J. Biol. Chem. 267*, 19418−19426.
13. DeVito, J., and Das, A. (1994) Control of transcription processivity in phage λ: Nus factors strengthen the termination-resistant state of RNA polymerase induced by N antiterminator, *Proc. Natl. Acad. Sci. U.S.A. 91*, 8660−8664.

14. Friedman, D. I., Olson, E. R., Johnson, L. L., Alessi, D., and Craven, M. G. (1990) Transcription-dependent competition for a host factor: The function and optimal sequence of the phage λ boxA transcription antitermination signal, *Genes Dev. 4*, 2210−2222.

15. Greenblatt, J., Nodwell, J. R., and Mason, S. W. (1993) Transcriptional antitermination, *Nature 364*, 401−406.

16. Mogridge, J., Mah, T. F., and Greenblatt, J. (1995) A protein−RNA interaction network facilitates the template-independent cooperative assembly on RNA polymerase of a stable antitermination complex containing the λ N protein, *Genes Dev. 9*, 2831−2845.

17. Friedman, D. I., Olson, E. R., Georgopoulos, C., Tilly, K., Herskowitz, I., and Banuett, F. (1984) Interactions of bacteriophage and host macromolecules in the growth of bacteriophage λ, *Microbiol. Rev. 48*, 299−325.

18. Greenblatt, J., Mah, T. F., Legault, P., Mogridge, J., Li J., and Kay, L. E. (1998). Structure and mechanism in transcriptional antitermination by the bacteriophage λ N protein, *Cold Spring Harbor Symp. Quant. Biol. 63*, 327−336.

19. Tan, R., and Frankel, A. D. (1995) Structural variety of arginine-rich RNA-binding peptides, *Proc. Natl. Acad. Sci. U.S.A. 92*, 5282−5286.

20. Cilley, C. D., and Williamson, J. R. (1997) Analysis of bacteriophage N protein and peptide binding to boxB RNA using polyacrylamide gel coelectrophoresis (PACE), *RNA 3*, 57−67.

21. van Gilst, M. R., and von Hippel, P. H. (1997) Assembly of the N-dependent antitermination complex of phage λ: NusA and RNA bind independently to different unfolded domains of the N protein, *J. Mol. Biol. 274*, 160−173.

22. Legault, P., Li, J., Mogridge, J., Kay, L. E., and Greenblatt, J. (1998) NMR structure of the bacteriophage λ N peptide/boxB RNA complex: Recognition of a GNRA fold by an arginine-rich motif, *Cell 93*, 289−299.

23. Scharpf, M., Sticht, H., Schweimer, K., Boehm, M., Hoffmann, S., and Rosch, P. (2000) Antitermination in bacteriophage λ. The structure of the N36 peptide−boxB RNA complex, *Eur. J. Biochem. 267*, 2397−2408.

24. Xia, T., Frankel, A., Takahashi, T. T., Ren, J., and Roberts, R. W. (2003) Context and conformation dictate function of a transcription antitermination switch, *Nat. Struct. Biol. 10*, 812−819.

25. Mah, T. F., Li, J., Davidson, A. R., and Greenblatt, J. (1999) Functional importance of regions in *Escherichia coli* elongation factor NusA that interact with RNA polymerase, the bacteriophage λ N protein and RNA, *Mol. Microbiol. 34*, 523−537.

26. Eisenmann, A., Schwarz, S., Prasch, S., Schweimer, K., and Rosch, P. (2005) The *E. coli* NusA carboxy-terminal domains are structurally similar and show specific RNAP- and λN interaction, *Protein Sci. 14*, 2018−2029.

27. Bonin, I., Muhlberger, R., Bourenkov, G. P., Huber, R., Bacher, A., Richter, G., and Wahl, M. C. (2004) Structural basis for the interaction of *Escherichia coli* NusA with protein N of phage λ, *Proc. Natl. Acad. Sci. U.S.A. 101*, 13762−13767.

28. Chattopadhyay, S., Hung, S. C., Stuart, A. C., Palmer, A. G., III, Garcia-Mena, J., Das, A., and Gottesman, M. E. (1995) Interaction between the phage HK022 Nun protein and the *nut* RNA of phage λ, *Proc. Natl. Acad. Sci. U.S.A. 92*, 12131−12135.

29. Mason, S. W., and Greenblatt, J. (1991). Assembly of transcription elongation complexes containing the N protein of phage λ and the *Escherichia coli* elongation factors NusA, NusB, NusG, and S10, *Genes Dev. 5*, 1504−1512.

30. Barik, S., Ghosh, B., Whalen, W., Lazinski, D., and Das, A. (1987) An antitermination protein engages the elongating transcription apparatus at a promoter-proximal recognition site, *Cell 50*, 885−899.

31. Kohno, T., Kusunoki, H., Sato, K., and Wakamatsu, K. (1998) A new general method for the biosynthesis of stable isotope-enriched peptides using a decahistidine-tagged ubiquitin fusion system: An application to the production of mastoparan-X uniformly enriched with ^{15}N and ^{15}N/^{13}C, *J. Biomol. NMR 12*, 109−121.

32. Marley, J., Lu, M., and Bracken, C. (2001) A method for efficient isotopic labeling of recombinant proteins, *J. Biomol. NMR 20*, 71−75.

33. Bax, A., and Grzesiek, S. (1993) Methodological advances in protein NMR, *Acc. Chem. Res. 26*, 131−138.

34. Schleucher, J., Schwendinger, M., Sattler, M., Schmidt, P., Schedletzky, O., Glaser, S. J., Sorensen, O. W., and Griesinger, C. (1994) A general enhancement scheme in heteronuclear multidimensional NMR employing pulsed field gradients, *J. Biomol. NMR 4*, 301−306.

35. Hajduk, P. J., Dinges, J., Miknis, G. F., Merlock, M., Middleton, T., Kempf, D. J., Egan, D. A., Walter, K. A., Robins, T. S., Shuker, S. B., Holzman, T. F., and Fesik, S. W. (1997) NMR-based discovery of lead inhibitors that block DNA binding of the human papillomavirus E2 protein, *J. Med. Chem. 40*, 3144−3150.

36. Wishart, D. S., and Sykes, B. D. (1994) Chemical shifts as a tool for structure determination, *Methods Enzymol. 239*, 363−392.

37. Daughdrill, G. W., Hanely, L. J., and Dahlquist, F. W. (1998) The C-terminal half of the anti-σ factor FlgM contains a dynamic equilibrium solution structure favoring helical conformations, *Biochemistry 37*, 1076−1082.

38. Wuthrich, K., Billeter, M., and Braun, W. (1984) Polypeptide secondary structure determination by nuclear magnetic resonance observation of short proton−proton distances, *J. Mol. Biol. 180*, 715−740.

39. Wagner, G., Neuhaus, D., Worgotter, E., Vasak, M., Kagi, J. H., and Wuthrich, K. (1986) Nuclear magnetic resonance identification of "half-turn" and 3(10)-helix secondary structure in rabbit liver metallothionein-2, *J. Mol. Biol. 187*, 131−135.

40. Pawley, N. H., Wang, C., Koide, S., and Nicholson, L. K. (2001) An improved method for distinguishing between anisotropic tumbling and chemical exchange in analysis of ^{15}N relaxation parameters, *J. Biomol. NMR 20*, 149−165.

41. Johnson, N. P., Baase, W. A., and von Hippel, P. H. (2005) Low energy CD of RNA hairpin unveils a loop conformation required for λN antitermination activity, *J. Biol. Chem. 280*, 32177−32183.

42. Koradi, R., Billeter, M., and Wuthrich, K. (1996) MOLMOL: A program for display and analysis of macromolecular structures, *J. Mol. Graphics 14*, 51−5, 29−32.